Electronic Supplementary Material (ESI) for Soft Matter.
This journal is © The Royal Society of Chemistry 2021

# Supporting Information

# Translational and rotational diffusion coefficients of gold nanorods functionalized with a high molecular weight, thermoresponsive ligand: A depolarized dynamic light scattering study

*Déborah Feller,[1] Marius Otten,[1] Marco Hildebrandt,[1] Marcel Krüsmann,[1] Gary Bryant,[2] Matthias Karg[1*]*

[1]Physikalische Chemie I: Kolloide und Nanooptik, Heinrich-Heine-Universität Düsseldorf, 40225 Düsseldorf, Germany

[2]Physics, School of Science, RMIT University, Melbourne, Victoria 3001, Australia

**TEM analysis of AuNR-PNIPAM samples**

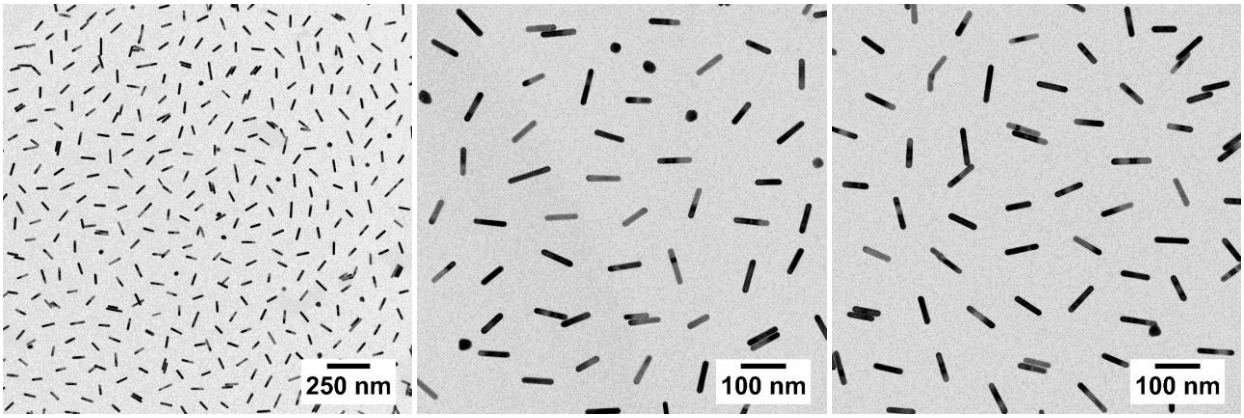


**Figure S1.** TEM images of AuNR-PNIPAM-1 at low magnifications.

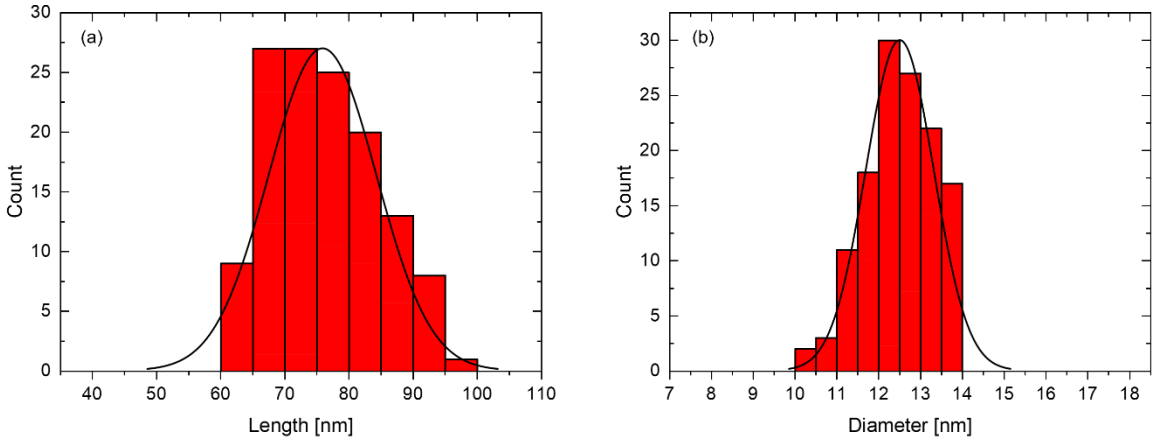


**Figure S2.** Size distribution histograms for length $L$ (a) and diameter $2R$ (b) of AuNR-PNIPAM-1 obtained from analysis of 130 individual particles from several TEM images. The black solid lines represent the fit to the data using gaussian size distributions.

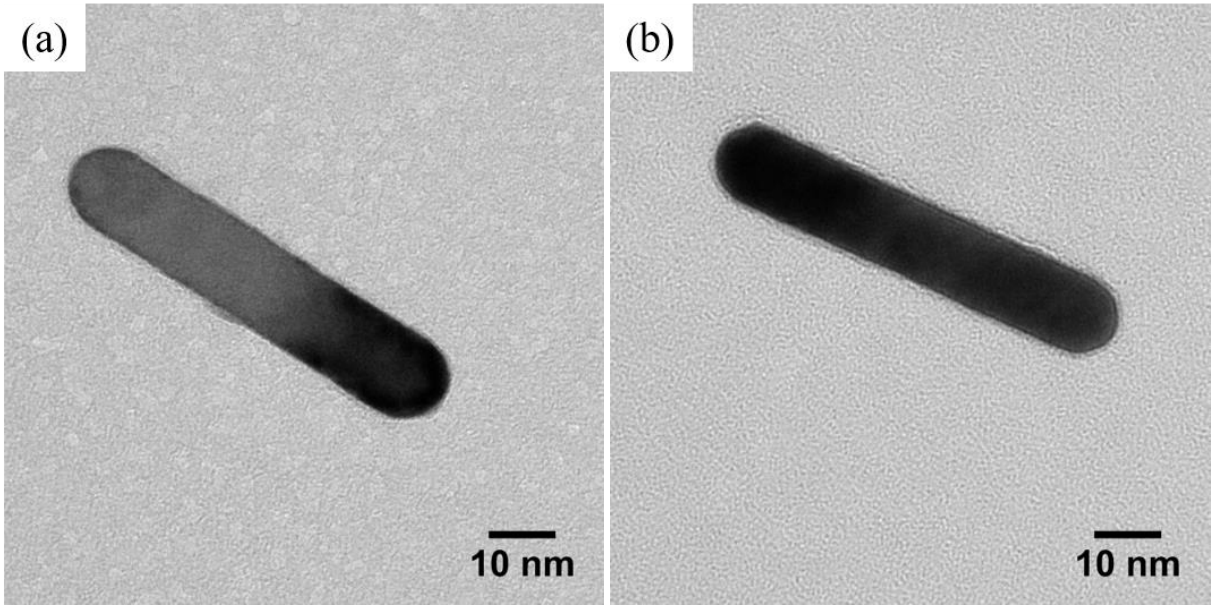


**Figure S3.** High magnification TEM images of AuNR-PNIPAM-1 particles. The collapsed PNIPAM shell surrounding the gold nanorods is partially visible.

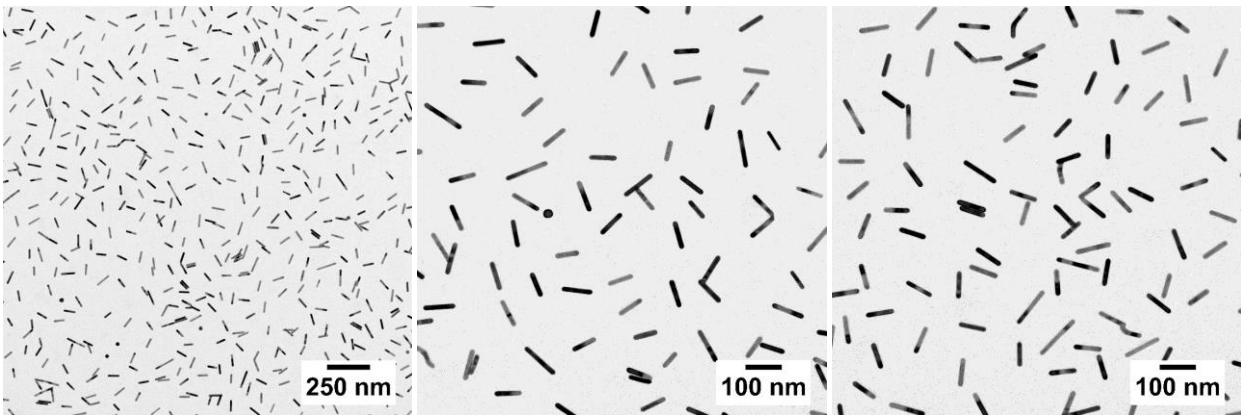


**Figure S4.** TEM images of AuNR-PNIPAM-2 at low magnifications.

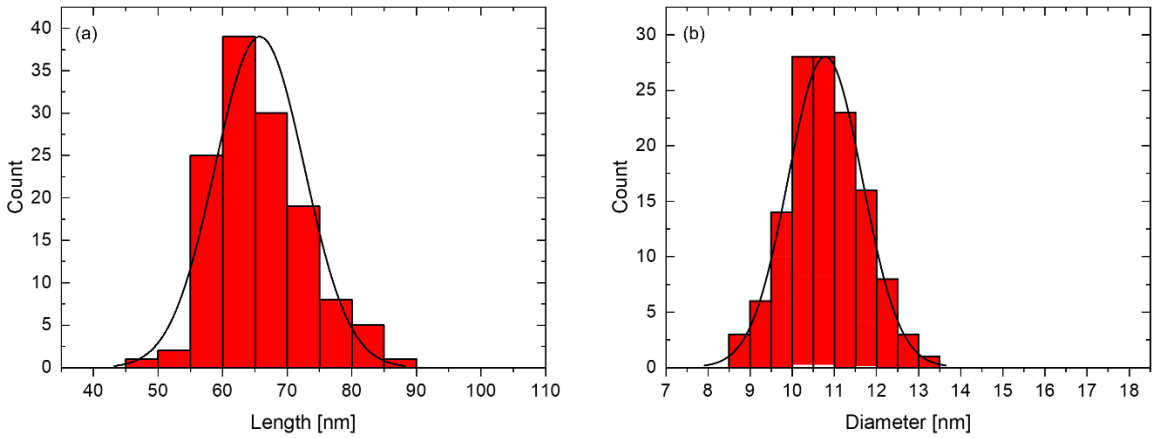


**Figure S5.** Size distribution histograms for length *L* (a) and diameter 2*R* (b) of AuNR-PNIPAM-2 obtained from analysis of 130 individual particles from several TEM images. The black solid lines represent the fit to the data using gaussian size distributions.

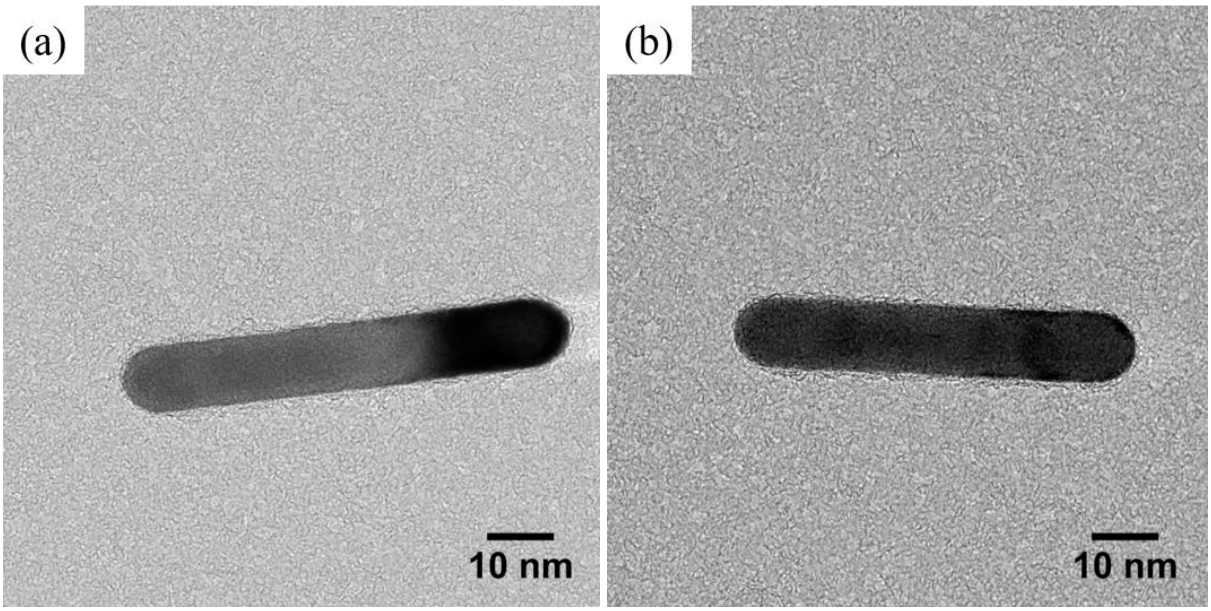


**Figure S6.** High magnification TEM images of AuNR-PNIPAM-2 particles. The collapsed PNIPAM shell surrounding the gold nanorods is partially visible.

**SAXS analysis of AuNR-PNIPAM samples**

In a typical SAXS experiment, scattered x-rays from a sample are detected by a position sensitive 2D detector. Via radial averaging of the detected signal, a 1D scattering curve is obtained. The scattering contrast in SAXS is determined by the electron density of the probed sample - in our case PNIPAM-functionalized gold nanoparticles in water. The scattering vector $\vec{q}$ defines the spatial resolution of the experiment. The magnitude of the scattering vector can be determined using:

$$|\vec{q}| = q = \frac{4\pi n}{\lambda} sin\left(\frac{\theta}{2}\right) \tag{S.1}$$

For x-rays $n = 1$, $\lambda$ refers to the wavelength of the incident radiation and $\theta$ to the scattering angle. Since $\lambda$ is typically small in x-ray scattering experiments, i.e. 0.154 nm in our experiment, SAXS probes larger values of $q$ than light scattering and thus resolves smaller structural features.

The average scattered intensity $I(q)$ is generally given by:

$$I(q) = N \cdot V^2 \cdot (\Delta\rho)^2 \cdot P(q) \cdot S(q) + I_B \tag{S.2}$$

Here $N$ is the particle number density, $\Delta\rho$ the contrast between the scattering object and the surrounding medium, $P(q)$ the form factor, $S(q)$ the structure factor and $I_B$ is related to incoherent background scattering. In the dilute state $S(q) \approx 1$. Because of the large contrast difference between gold and the PNIPAM ligands with respect to water as dispersion medium, the measured SAXS profiles are dominated by scattering from the gold particles.

To describe the experimental scattering data for our gold nanorod samples (AuNR-PNIPAM), we used the form factor of a simple cylinder:[1-3]

$$P(q) = 16 \int_0^1 \left(\frac{J_1\left(qR\sqrt{1-x^2}\right) sin(qLx/2)}{q^2 R\sqrt{1-x^2}Lx}\right)^2 dx \tag{S.3}$$

Here $J_n(x)$ are the regular cylindrical Bessel functions of order $n$, $R$ is the radius and $L$ the length of the cylinder. To account for polydispersity, the form factor was convoluted with a normalized gaussian distribution function:

$$D\left(R, \langle R\rangle, \sigma_{poly}\right) = \frac{1}{\sqrt{2\pi\sigma_{poly}{}^2}} exp\left(\frac{-(R-\langle R\rangle)^2}{2\sigma_{poly}{}^2}\right) \tag{S.4}$$

Here $<R>$ denotes the average particle radius and $\sigma_{poly}$ represents the relative particle size polydispersity.

The scattering data of both samples and the corresponding cylinder fits are shown in **Figure S7**.

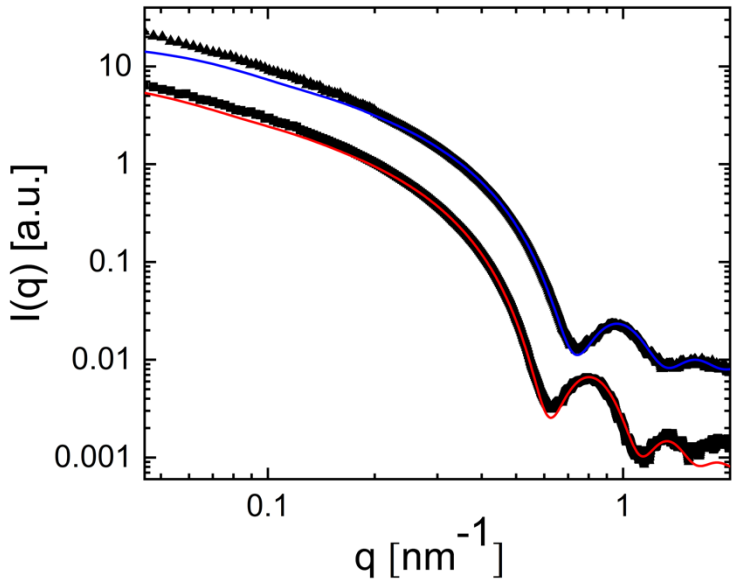


**Figure S7.** SAXS profiles for AuNR-PNIPAM-1 (squares and red solid line) and AuNR-PNIPAM-2 (triangles and blue solid line). The profile and fit for AuNR-PNIPAM-2 have been shifted vertically for clarity. The solid lines are fits using equation S.3 taking into account Gaussian polydispersity (S.4).

This simple form factor model describes the scattering profiles sufficiently well albeit with some minor deviations in the low $q$ region. This deviation is attributed to a small fraction of aggregates in the samples. To account for these aggregates, a fractal model was applied.[4] The corresponding fits to the data are shown in the main manuscript. We want to highlight that this fractal contribution does not affect the radius obtained from the cylinder model. Due to pronounced form factor minima in the high $q$ region, the radius can be determined very reliably and with small error. Because of the limited $q$ range at low $q$, the length obtained from the cylinder model is less reliable.

**Optical properties of the AuNR-PNIPAM particles**

The temperature induced PNIPAM collapse on the surface of the gold nanorods can be monitored by extinction spectroscopy because of the resulting change in local refractive index in the vicinity of the gold nanoparticle surface. **Figures S8,9** show the resulting redshift of the longitudinal LSPRs of the AuNRs with increasing temperature.

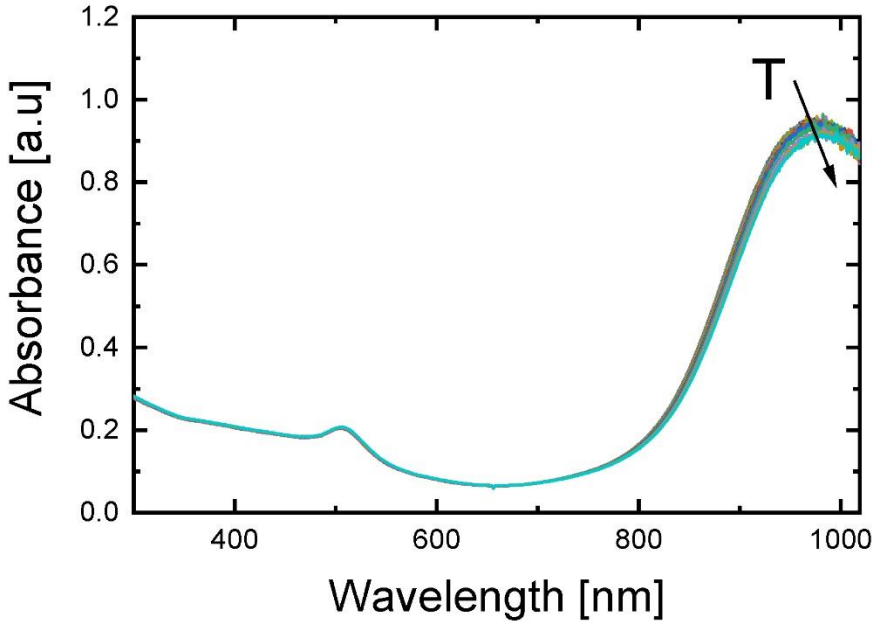


**Figure S8.** UV/Vis-spectra of AuNR-PNIPAM-1 measured in dilute aqueous dispersion. Spectra were recorded in a temperature range from 15 °C to 33°C in steps of 1°C.

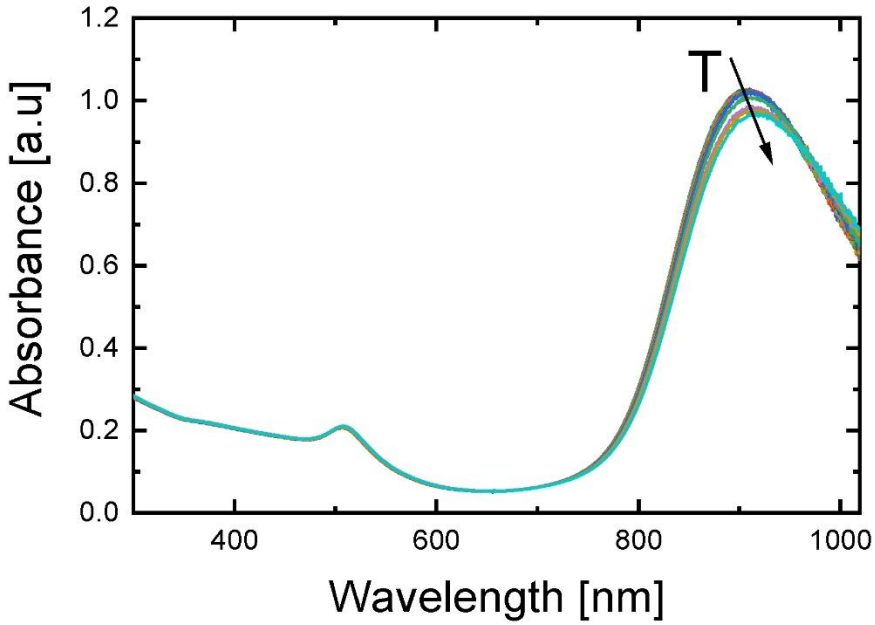


**Figure S9.** UV/Vis-spectra of AuNR-PNIPAM-2 measured in dilute aqueous dispersion. Spectra were recorded in a temperature range from 15 °C to 33°C in steps of 1°C.

**DLS and DDLS analysis of the AuNR-PNIPAM samples**

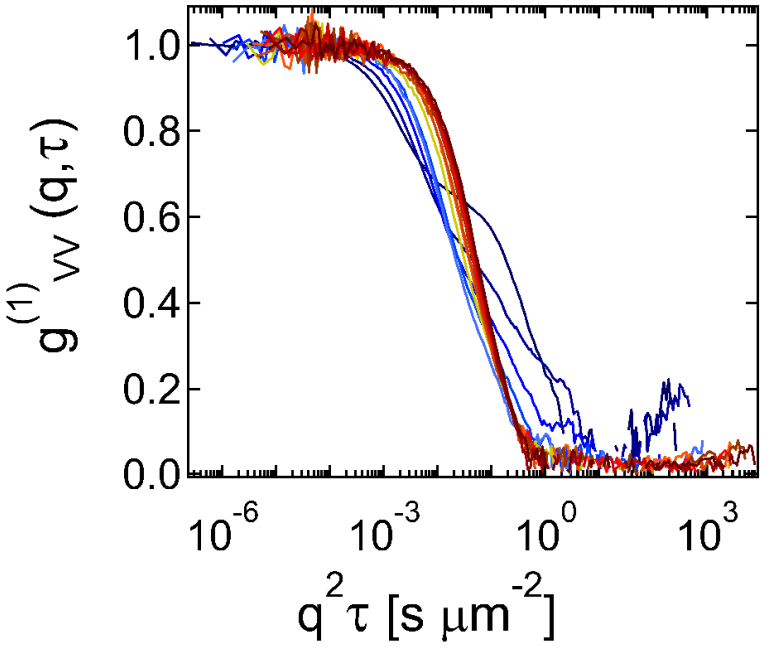


**Figure S10**. $g^{(1)}_{VV}$ recorded at scattering angles between 20° to 140° in 10° steps plotted against $q^2\tau$ for AuNR-PNIPAM-1. The scattering angle increases from blue to red.

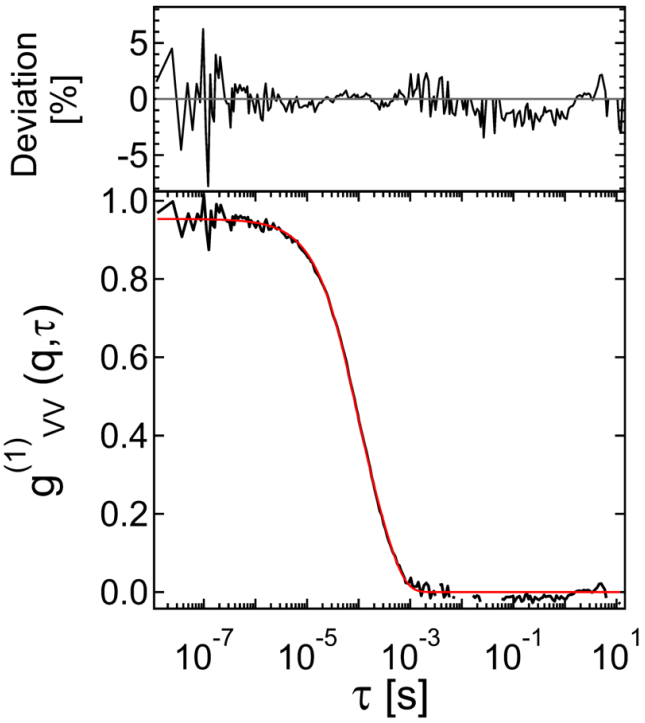


**Figure S11.** $g^{(1)}_{VV}(q,\tau)$ (black) and the corresponding fit (red) for AuNR-PNIPAM-1 recorded at 120°. The small deviation between the experimental curve and the fit is shown in the top graph.

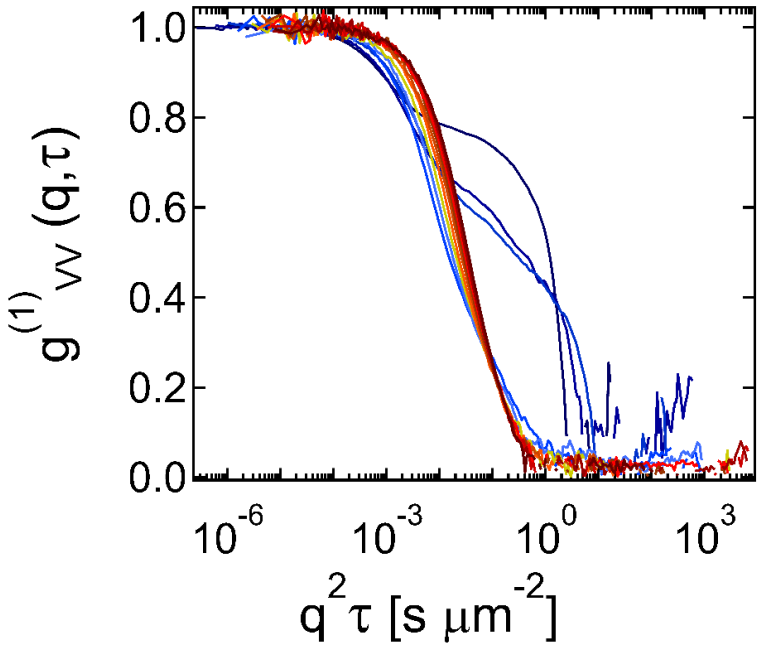


**Figure S12.** $g^{(1)}_{VV}$ recorded at scattering angles between 20° to 140° in 10° steps plotted against $q^2\tau$ for AuNR-PNIPAM-2. The scattering angle increases from blue to red.

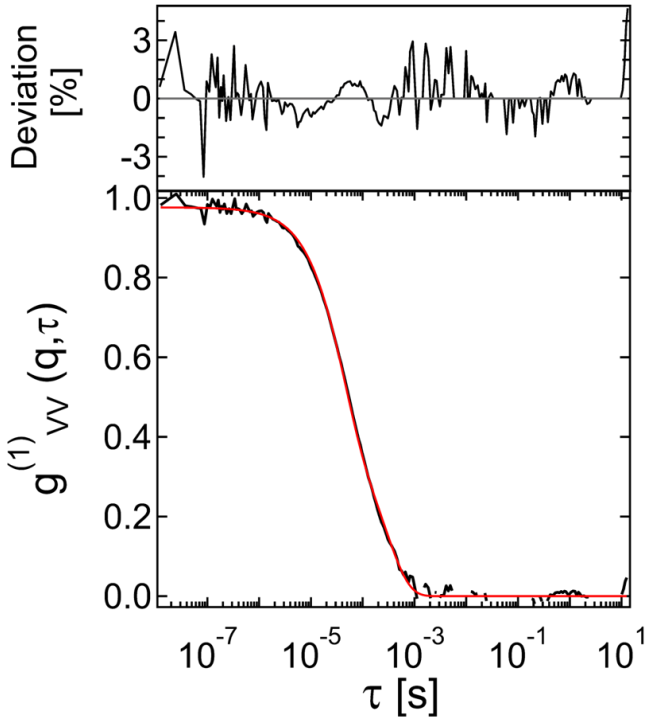


**Figure S13.** $g^{(1)}_{VV}(q,\tau)$ (black) and the corresponding fit (red) for AuNR-PNIPAM-2 recorded at 120°. The small deviation between the experimental curve and the fit is shown in the top graph.

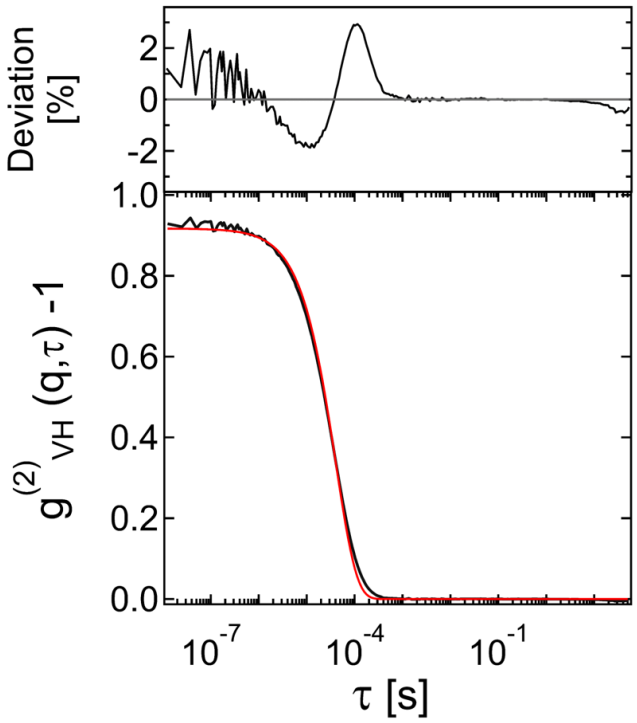


**Figure S14.** $g^{(2)}_{VH}(q,\tau) - 1$ (black) and the corresponding fit (red) of AuNR-PNIPAM-1 recorded at 120°. The deviation between the experimental curve and the fit is shown in the top graph.

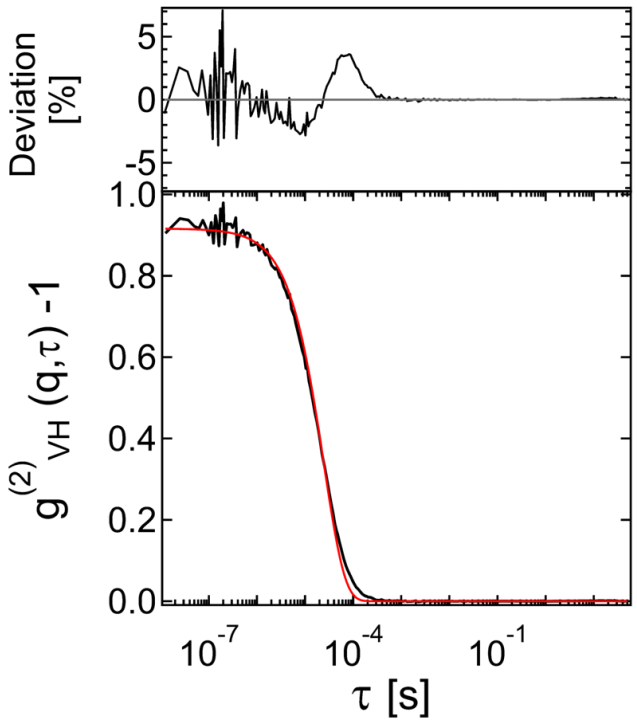


**Figure S15.** $g^{(2)}_{VH}(q,\tau) - 1$ (black) and the corresponding fit (red) of AuNR-PNIPAM-2 recorded at 120°. The deviation between the experimental curve and the fit is shown in the top graph.

**Analysis of PNIPAM ligand**

The $^{1}$H-NMR spectrum of the PNIPAM ligand is shown in **Figure S16**.

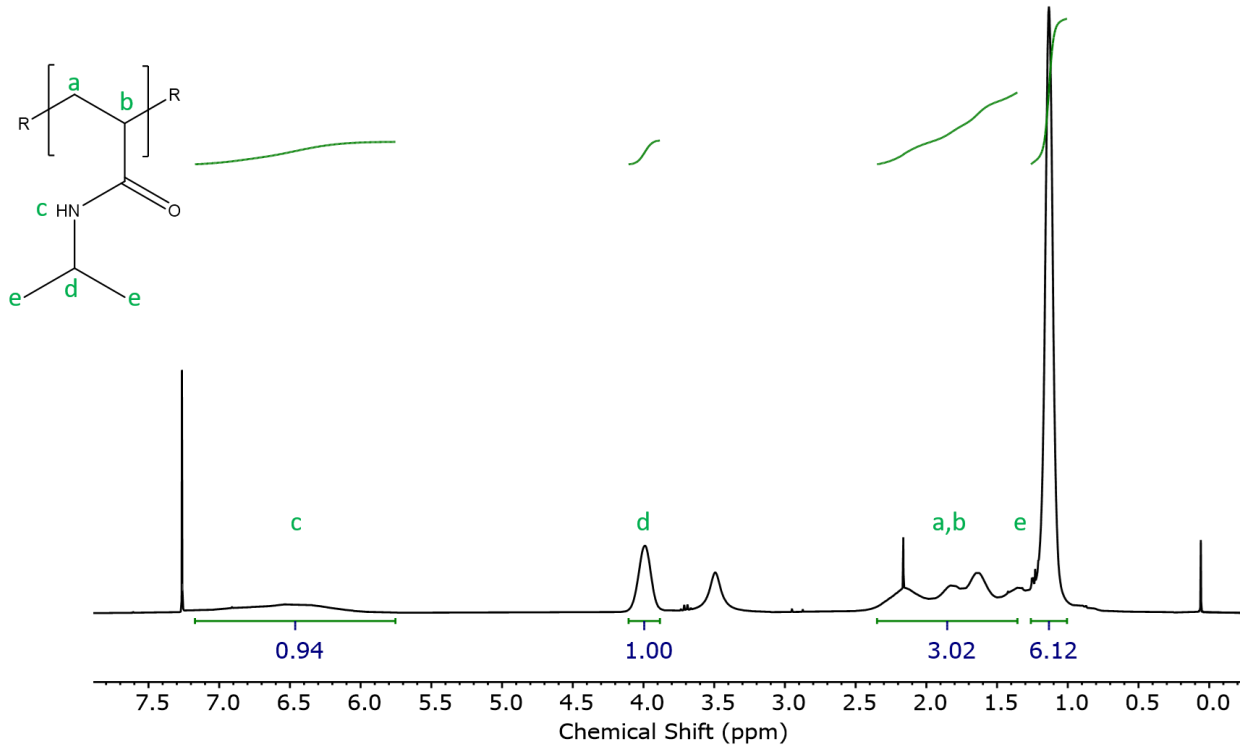


**Figure S16.** $^{1}$H-NMR spectrum of PNIPAM recorded in $CDCl_3$. Chemical Shifts (ppm): 7.17-5.57 (c, NH, s), 3.98 (d, -NCH, s), 2.35-1.36 (a, b, polymer backbone, m), 1.12 (e, -$CH_3$, t).

The molecular weight of the ligand determined (monomer consumption) is $M_n$ = 85,000 g/mol. The peaks at chemical shifts of 3.5 ppm, 2.2 ppm and 1.32 ppm are attributed to the solvent used during the synthesis. The sharp peak at 0.06 ppm can be attributed to silicon grease.

In addition to NMR, we analyzed the PNIPAM ligand by GPC providing an average PDI of 1.69. The PDI and $M_n$ give access to the molecular weight $M_w$ of the PNIPAM ligand:

$$M_w = M_n \cdot 1.69 = 85000 \frac{g}{mol} \cdot 1.69 = 143650 \frac{g}{mol} \quad \text{(S.5)}$$

**Theoretical calculations of the PNIPAM brush thickness**

In order to estimate the expected brush thickness $T$ for our PNIPAM ligand on the gold nanoparticle surface we use the theoretical end-to-end distance $R$:[5]

$$R = L_K \cdot {N_K}^{\nu} \tag{S.6}$$

where $L_K$ is the Kuhn length, $\nu$ defines the solvent quality and $N_K$ is the number of Kuhn segments:

$$N_K = \frac{N \cdot b}{L_K} \tag{S.7}$$

Here $b$ corresponds to the monomer length and $N$ is the degree of polymerization. $N$ can be calculated from the respective molecular weights of the polymer and the monomer units:

$$N = \frac{M_w}{M(NIPAM)} = \frac{143650 \frac{g}{mol}}{113.16 \frac{g}{mol}} = 1269 \tag{S.8}$$

Considering a low grafting density of the PNIPAM ligand on the gold surface, the theoretical brush thickness can be estimated as:

$$T \geq 2R_g \tag{S.9}$$

where $R_g$ is the radius of gyration that is accessible from the end-to-end distance $R$:

$$\langle {R_g}^2 \rangle = \frac{\langle R^2 \rangle}{6} \tag{S.10}$$

The brush thickness $T$ is calculated using the equations S.6, S.9 and S.10. The results and used constants are summarized in **Table S1**.

**Table S1.** Constants and results of the calculation for the theoretical brush thickness $T$.

| | |
|---|---|
| $\boldsymbol{\nu}$ | 0.59 |
| $\boldsymbol{L_K}$ | 4 nm[5] |
| $\boldsymbol{b}$ | 0.25 nm |
| $\boldsymbol{N_K}$ | 79 |
| $\boldsymbol{R}$ | 52.8 nm |
| $\boldsymbol{R_g}$ | 21.6 nm |
| $\boldsymbol{T}$ | 43.2 nm |

**Preparation of spherical gold nanoparticles and decoration with PNIPAM ligand (AuNS-PNIPAM)**

Spherical gold nanoparticles (AuNS) were synthesized following the well-known protocol of Turkevich et al.[6] The as prepared AuNS were stabilized by citrate in dilute aqueous dispersion. Ligand exchange with PNIPAM at room temperature was done as follows: 2 mg PNIPAM were dissolved in 800 µL Milli-Q water and 0.1 mg of $NaBH_4$ was added. The solution was stirred for 10 minutes and then added dropwise to 3 mL of the aqueous AuNP solution (0.061 M). The solution was stirred for 100 hours. Afterwards the sample was centrifuged at 5400 rcf for 2 h 30 min at 20 °C. The clear and colourless supernatant was removed and the residue (AuNS-PNIPAM) was dispersed in 3 mL of Milli-Q water.

Prior to the DLS experiments, 0.2 ml of AuNS-PNIPAM solution were diluted with 1.8 mL Milli-Q water and the pH was adjusted to 7 using a dilute NaOH solution. At that pH it is ensured that the terminating carboxyl groups of the ligand are deprotonated and thus electrostatic repulsion between the particles is maximized. The solution was filtered with a 5 µm PTFE hydrophobic syringe filter and directly filled into a quartz-glass cuvette.

**Characterization of AuNS-PNIPAM**

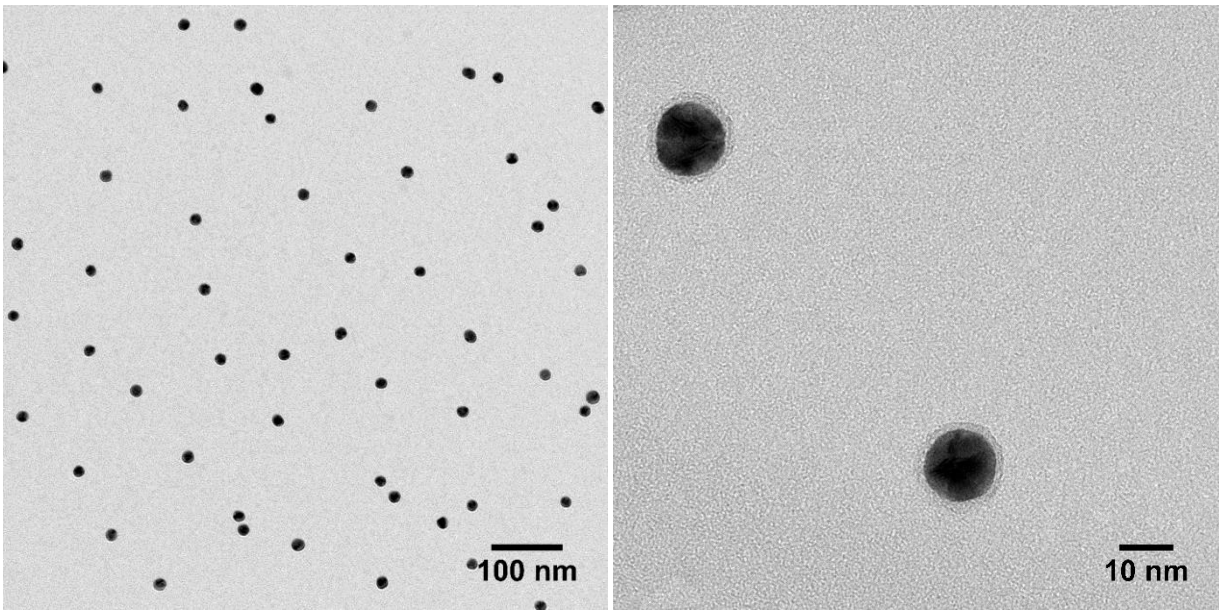


**Figure S17.** TEM images of AuNS-PNIPAM at different magnifications. The collapsed PNIPAM shell homogeneously surrounding the gold spheres is clearly visible in the image on the right.

The size, shape and polydispersity of the AuNS-PNIPAM particles was also studied by SAXS. The scattering data were described with the form factor of hard spheres with the sphere radius $R$:

$$P(q) = \left[3\frac{sin(qR)-qRcos(qR)}{(qR)^3}\right]^2 \quad \text{(S.11)}$$

**Figure S18** shows the scattering data and the corresponding fit.

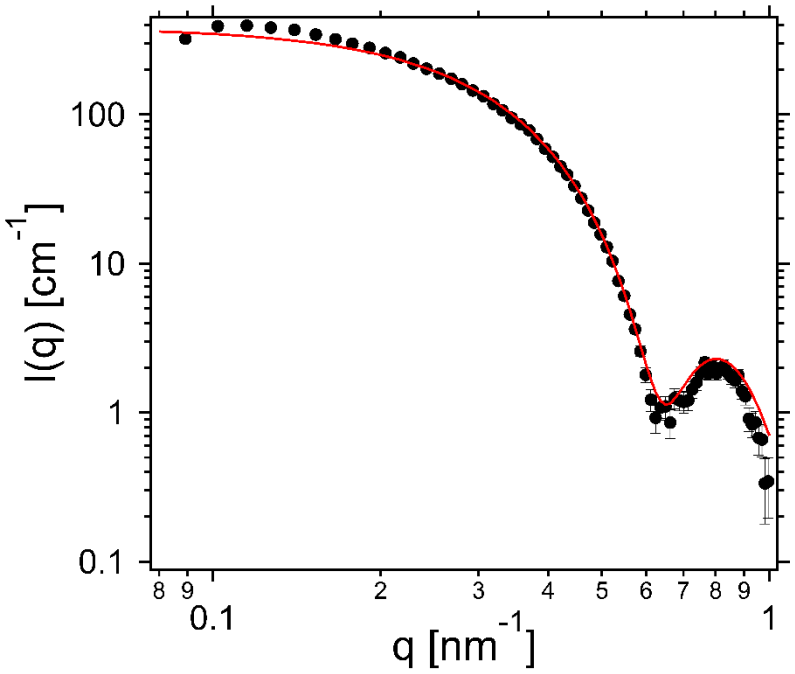


**Figure S18.** Experimental SAXS profile of AuNS-PNIPAM (symbols) with the respective fit using a polydisperse sphere model (red).

The fit yields an average particle radius of $R$ = 6.89 ± 0.06 nm.

Due to large contrast difference between PNIPAM shell and the gold cores, SAXS is not suitable to determine the thickness of the ligand shell. Therefore, we measured DLS of the AuNS-PNIPAM particles in dilute aqueous dispersion. Measurements were performed at a scattering angle of 90° within the same temperature range as for the gold rods. **Figure S19** shows a representative intensity-time autocorrelation function recorded at 25 °C.

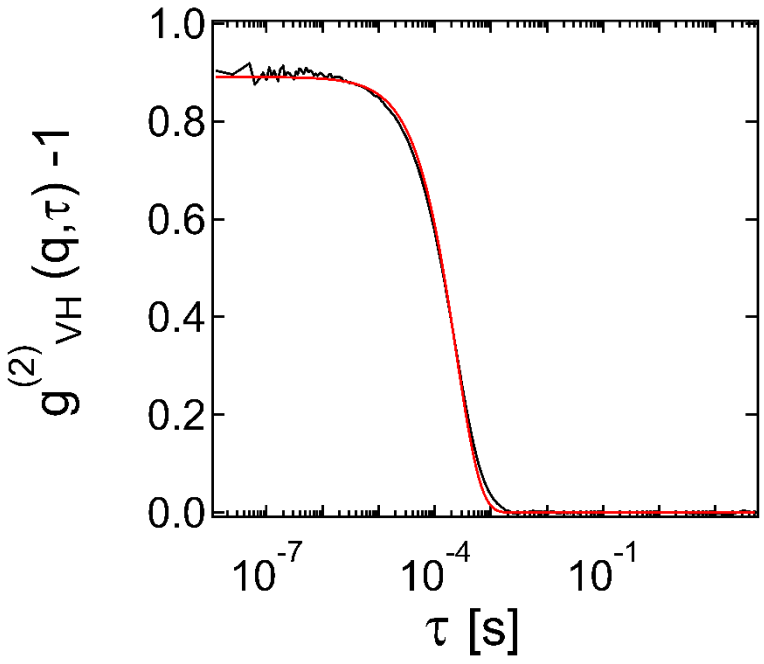


**Figure S19.** Correlation function (black) of AuNS-PNIPAM recorded at a scattering angle of 90° at 25 °C shown with a single exponential fit (red).

The correlation function was fitted using a single exponential fit (see equation 4, main manuscript) to extract the decay rate $\Gamma$. For each temperature $\Gamma$ was determined from three individual measurements and then used to calculate hydrodynamic radii $R_h$ based on equations 5 and 7 from the main manuscript. The brush thickness $T$ was determined using the values of $R_h$ and taking into account the average radius of the AuNS cores as determined from SAXS (6.89 ± 0.06 nm). The resulting values for each temperature are listed in **Table S2**.

**Table S2.** Hydrodynamic radii of AuNS-PNIPAM for each measured temperature and the resulting brush thickness *T*.

| **Temperature [°C]** | $R_h$ **[nm]** | $T$ **[nm]** |
|---|---|---|
| **25** | 41.4 ± 0.2 | 34.5 ± 0.1 |
| **27** | 42.4 ± 0.3 | 35.6 ± 0.2 |
| **29** | 41.2 ± 0.4 | 34.3 ± 0.3 |
| **30** | 40.6 ± 0.5 | 33.7 ± 0.3 |
| **31** | 40.5 ± 0.2 | 33.6 ± 0.1 |
| **32** | 39.2 ± 0.2 | 32.3 ± 0.1 |
| **33** | 38.0 ± 0.4 | 31.1 ± 0.3 |
| **34** | 36.4 ± 0.2 | 29.5 ± 0.1 |
| **35** | 35.1 ± 0.3 | 28.2 ± 0.2 |
| **37** | 32.1 ± 0.2 | 25.2 ± 0.1 |
| **39** | 30.2 ± 0.1 | 23.3 ± 0.1 |

Due to the change in local refractive index in the vicinity of the gold nanoparticle surface, the ligand exchange and temperature induced PNIPAM collapse can also be monitored by extinction spectroscopy. **Figure S20** shows the resulting changes to the LSPR of the AuNS and AuNS-PNIPAM particles.

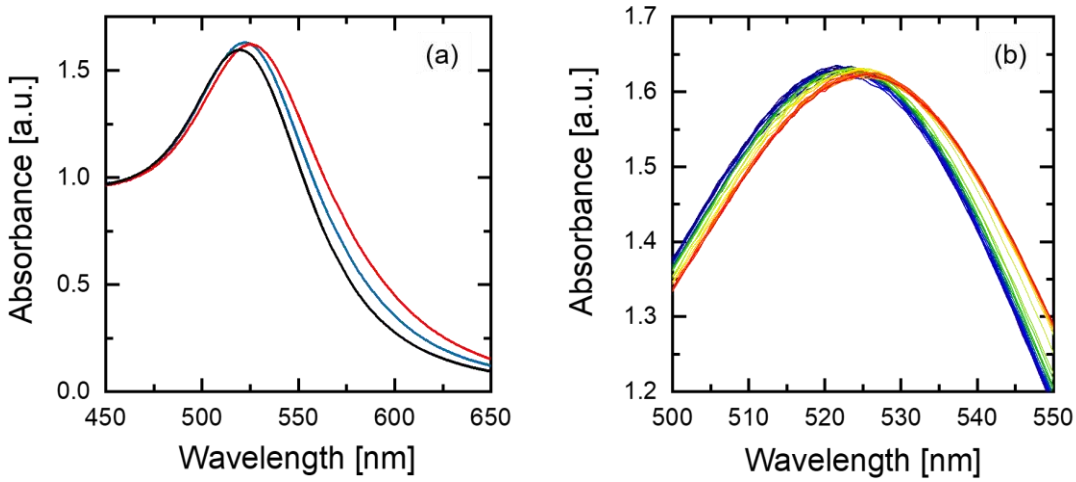


**Figure S20.** (a) UV/Vis-spectra of citrate-stabilized AuNS (black), AuNS-PNIPAM at 15 °C (blue) and at 40 °C (red). (b) Localized surface plasmon resonance (LSPR) peak maximum of AuNS-PNIPAM with increasing temperature from blue (15°C) to red (40°C) in steps of 1°C.

**Temperature dependence of the diffusion coefficients**

**Tables S3 and S4** list the experimentally determined diffusion coefficients from DLS and DDLS measurements performed at different temperatures below and close to the LCST of the PNIPAM ligands. The theoretical values were calculated using equations 14-18 from the main manuscript and using the temperature dependent brush thickness *T* determined for the spherical reference particles (see **table S2**). The deviation between experiment and theory is represented by the calculated ratios (experimental values divided by theoretical ones).

**Table S3**. Experimental and theoretical values for $D_t$ and $D_r$ and the ratios *r* for the sample AuNR-PNIPAM-1.

| **Temperature [°C]** | **Experiment** | | **Theory** | | **ratio (Exp/Theo)** | |
|---|---|---|---|---|---|---|
| | $D_t$ **[µm²/s]** | $D_r$ **[1/ms]** | $D_t$ **[µm²/s]** | $D_r$ **[1/ms]** | $r(D_t)$ | $r(D_r)$ |
| **25** | 5.68 ± 0.10 | 1.54 ± 0.03 | 4.82 ± 0.23 | 1.48 ± 0.27 | 1.18 | 1.04 |
| **27** | 5.77 ± 0.03 | 1.83 ± 0.04 | 4.98 ± 0.23 | 1.48 ± 0.28 | 1.16 | 1.23 |
| **29** | 6.51 ± 0.05 | 2.19 ± 0.04 | 5.34 ± 0.26 | 1.65 ± 0.31 | 1.22 | 1.33 |
| **30** | 7.46 ± 0.05 | 2.39 ± 0.04 | 5.56 ± 0.28 | 1.75 ± 0.32 | 1.34 | 1.37 |
| **31** | 8.41 ± 0.03 | 2.70 ± 0.02 | 5.71 ± 0.28 | 1.80 ± 0.32 | 1.47 | 1.50 |
| **32** | 8.58 ± 0.01 | 3.00 ± 0.03 | 6.00 ± 0.31 | 1.97 ± 0.34 | 1.43 | 1.53 |
| **33** | 8.65 ± 0.02 | 3.11 ± 0.03 | 6.32 ± 0.35 | 2.15 ± 0.37 | 1.37 | 1.45 |

**Table S4.** Experimental and theoretical values for $D_t$ and $D_r$ and the ratios $r$ from experiment to theory for the sample AuNR-PNIPAM-2.

| Temperature [°C] | Experiment | | Theory | | ratio (Exp/Theo) | |
|---|---|---|---|---|---|---|
| | $D_t$ [µm²/s] | $D_r$ [1/ms] | $D_t$ [µm²/s] | $D_r$ [1/ms] | $r(D_t)$ | $r(D_r)$ |
| **25** | 6.46 ± 0.25 | 2.75 ± 0.06 | 5.05 ± 0.29 | 1.79 ± 0.25 | 1.28 | 1.54 |
| **27** | 6.83 ± 0.26 | 3.21 ± 0.05 | 5.21 ± 0.30 | 1.79 ± 0.26 | 1.31 | 1.80 |
| **29** | 6.91 ± 0.22 | 3.82 ± 0.13 | 5.59 ± 0.34 | 1.99 ± 0.28 | 1.24 | 1.92 |
| **30** | 7.54 ± 0.22 | 4.93 ± 0.10 | 5.83 ± 0.37 | 2.11 ± 0.30 | 1.29 | 2.33 |
| **31** | 9.25 ± 0.18 | 5.01 ± 0.04 | 5.98 ± 0.36 | 2.18 ± 0.29 | 1.55 | 2.30 |
| **32** | 9.67 ± 0.20 | 5.25 ± 0.08 | 6.30 ± 0.40 | 2.39 ± 0.31 | 1.53 | 2.20 |
| **33** | 9.78 ± 0.04 | 5.57 ± 0.06 | 6.64 ± 0.46 | 2.62 ± 0.35 | 1.47 | 2.13 |
| **34** | 9.83 ± 0.02 | 5.98 ± 0.07 | 7.05 ± 0.50 | 2.94 ± 0.36 | 1.39 | 2.04 |
| **35** | 9.91 ± 0.07 | 6.22 ± 0.08 | 7.42 ± 0.56 | 3.22 ± 0.39 | 1.33 | 1.93 |

## References


[1] J. Pedersen, *Adv. Colloid Interface Sci.*, 1997, **70**, 171-210.
[2] G. Fournet, *Bull. Soc. Fr. Mineral. Cristallogr.*, 1951, **74**, 39-113.
[3] L. Onsager, *Ann. New York Acad. Sci.*, 1949, **51**, 627-659.
[4] J. Teixeira, *J. Appl. Cryst.*, 1988, **21**, 781–785.
[5] C. G. Lopez, A. Scotti, M. Brugnoni and W. Richtering, *Macromol. Chem. Phys.*, 2018, **12**, 1800421.
[6] J. Turkevich, P. C. Stevenson and J. Hillier, *Discuss. Faraday Soc.*, 1951, **11**, 55-75.